AFRL-RX-WP-TP-2009-4126

OXIDATION OF ZrB_2 AND ZrB_2-SiC CERAMICS WITH TUNGSTEN ADDITIONS (PREPRINT)

S.C. Zhang, W.G. Fahrenholtz, and G.E. Hilmas

University of Missouri-Rolla

FEBRUARY 2009

AIR FORCE RESEARCH LABORATORY
MATERIALS AND MANUFACTURING DIRECTORATE
WRIGHT-PATTERSON AIR FORCE BASE, OH 45433-7750
AIR FORCE MATERIEL COMMAND
UNITED STATES AIR FORCE

REPORT DOCUMENTATION PAGE

Form Approved
OMB No. 0704-0188

1. REPORT DATE *(DD-MM-YY)*	2. REPORT TYPE	3. DATES COVERED *(From - To)*
February 2009	Conference Paper Preprint	

4. TITLE AND SUBTITLE
OXIDATION OF ZrB_2 AND ZrB_2-SiC CERAMICS WITH TUNGSTEN ADDITIONS (PREPRINT)

5a. CONTRACT NUMBER
FA8650-04-C-5704

5b. GRANT NUMBER

5c. PROGRAM ELEMENT NUMBER
78011F

6. AUTHOR(S)
S.C. Zhang, W.G. Fahrenholtz, and G.E. Hilmas

5d. PROJECT NUMBER
2865

5e. TASK NUMBER
25

5f. WORK UNIT NUMBER
25100000

7. PERFORMING ORGANIZATION NAME(S) AND ADDRESS(ES)

University of Missouri-Rolla
1870 Miner Circle
Rolla, MO 65409-0970

Metals Branch (AFRL/RXLMP)
Metals, Ceramics, and NDE Division
Materials and Manufacturing Directorate
Wright-Patterson Air Force Base, OH 45433-7750
Air Force Materiel Command, United States Air Force

8. PERFORMING ORGANIZATION REPORT NUMBER

9. SPONSORING/MONITORING AGENCY NAME(S) AND ADDRESS(ES)
Air Force Research Laboratory
Materials and Manufacturing Directorate
Wright-Patterson Air Force Base, OH 45433-7750
Air Force Materiel Command
United States Air Force

10. SPONSORING/MONITORING AGENCY ACRONYM(S)
AFRL/RXLMP

11. SPONSORING/MONITORING AGENCY REPORT NUMBER(S)
AFRL-RX-WP-TP-2009-4126

12. DISTRIBUTION/AVAILABILITY STATEMENT
Approved for public release; distribution unlimited.

13. SUPPLEMENTARY NOTES
Conference paper submitted to the proceedings of the 214th meeting of the Electrochemical Society. PAO Case Number: 88 ABW-2008-1143; Clearance Date: 26 Nov 2008. Paper contains color.

14. ABSTRACT
The effect of tungsten additions on the oxidation behavior of zirconium diboride-based ceramics was studied. Four mole percent tungsten carbide was added to ZrB_2. The oxidation behavior was studied using thermal gravimetric analysis and isothermal testing in flowing air. Upon heating to 1500°C, the mass gain decreased from ~14 mg/cm^2 for nominally pure ZrB_2 to ~4.5 mg/cm^2 for tungsten containing ZrB_2. After heating to 1500°C for three hours, the scale thickness on nominally pure ZrB_2 was ~500 μm compared to ~100 μm for tungsten containing ZrB_2. Tungsten additions improved the oxidation resistance of ZrB_2 by modifying the morphology of the ZrO_2 scale by liquid phase sintering, making it a better barrier to oxygen diffusion.

15. SUBJECT TERMS
tungsten additions, zirconium diboride-based ceramics, ultra-high temperature ceramics (UHTCs)

16. SECURITY CLASSIFICATION OF:			17. LIMITATION OF ABSTRACT:	18. NUMBER OF PAGES	19a. NAME OF RESPONSIBLE PERSON (Monitor)
a. REPORT	b. ABSTRACT	c. THIS PAGE			Todd J. Turner
Unclassified	Unclassified	Unclassified	SAR	16	19b. TELEPHONE NUMBER *(Include Area Code)* N/A

For submission to proceedings of the 214th meeting of the Electrochemical Society

Oxidation of ZrB_2 and ZrB_2-SiC Ceramics with Tungsten Additions

S.C. Zhang, W.G. Fahrenholtz, and G.E. Hilmas

Materials Science and Engineering Department, Missouri University of Science and Technology, Rolla, 65409

The effect of tungsten additions on the oxidation behavior of zirconium diboride-based ceramics was studied. Four mole percent tungsten carbide was added to ZrB_2. The oxidation behavior was studied using thermal gravimetric analysis and isothermal testing in flowing air. Upon heating to 1500°C, the mass gain decreased from ~14 mg/cm^2 for nominally pure ZrB_2 to ~4.5 mg/cm^2 for tungsten containing ZrB_2. After heating to 1500°C for three hours, the scale thickness on nominally pure ZrB_2 was ~500 μm compared to ~100 μm for tungsten containing ZrB_2. Tungsten additions improved the oxidation resistance of ZrB_2 by modifying the morphology of the ZrO_2 scale by liquid phase sintering, making it a better barrier to oxygen diffusion.

Introduction

The borides, carbides, and nitrides of the early transition metals are considered ultra-high temperature ceramics (UHTCs) because they have melting temperatures above 3000°C. These materials have an unusual combination of strength at elevated temperature, high elastic modulus and hardness, high thermal and electrical conductivities, and stability in reactive environments (1,2). As such, UHTCs are candidates for applications involving extreme environments such as those associated with hypersonic flight, atmospheric re-entry, and rocket propulsion (3,4). In addition, these materials are under consideration for applications such as cutting tools, high temperature electrodes, microelectronic devices, nuclear fuel forms, and molten metal contact (5-9). More specifically for the present study, ZrB_2 has a combination of oxidation resistance and high thermal conductivity that makes it attractive for leading edges in hypersonic vehicles (3,10,11).

The oxidation resistance of nominally pure ZrB_2 varies with temperature. Below about 1000°C, a combination of porous, crystalline ZrO_2 and amorphous or liquid B_2O_3 forms on the surface (12,13). The B_2O_3 forms a continuous layer that acts as a barrier to oxygen diffusion resulting in parabolic mass gain kinetics. However, B_2O_3 has a low melting temperature (~450°C) and a relatively high vapor pressure (14,15). Between 1000°C and about 1200°C, the rates of B_2O_3 formation and evaporation are comparable, resulting in para-linear mass gain kinetics (16). At higher temperatures (1200°C and above), B_2O_3 evaporation is rapid. Loss of the protective layer allows for direct contact between the atmosphere and ZrB_2, which results in linear mass gain kinetics (17). Recently, Parthasarathy et al. have developed a mechanistic model that describes both the structural evolution and the rate-limiting steps at various stages of oxidation for ZrB_2, HfB_2, and TiB_2 (18,19).

Typically, oxidation resistance of the diborides is improved by adding compounds such as SiC, $MoSi_2$, or $TaSi_2$ that form a protective SiO_2-rich oxide scale at temperatures

above 1200°C (20-24). Compared to pure B_2O_3, borosilicate glasses are less volatile and provide a stable diffusion barrier during oxidation at intermediate temperatures (1200°C to 1600°C), which extends the temperature range for protective behavior (25). However, this approach only provides protection up to ~1600°C, not to the ultra-high temperatures that are predicted for hypersonic flight applications. At higher temperatures, loss of the SiO_2 scale again leaves a porous ZrO_2 scale on the surface of the diboride, resulting in rapid oxidation (26). In some cases, the ZrO_2 scale has been shown to densify, resulting in improved oxidation protection at temperatures of 1800°C or higher (26).

Some researchers have reported formation of a SiC-depleted layer beneath the surface borosilicate glass layer during oxidation of ZrB_2-SiC ceramics (20,21,27). This layer is thought to form due to active oxidation of SiC beneath the scale, which is caused by low oxygen activity below the diffusion barrier (28). Formation of a SiC-depleted layer is likely to be detrimental to stability of the scale at elevated temperatures due to the increase in pressure of species such as SiO and CO in the porous SiC-depleted layer, which could cause rupture of the SiO_2 scale (25,26).

The purpose of this research was to examine tungsten additions as a possible route to improve the oxidation resistance of ZrB_2 ceramics. The initial motivation to explore transition metal additions was based on the possibility of modifying the microstructure of the ZrO_2 scale (29). Specifically, WO_3 forms a eutectic with ZrO_2 at ~1275°C. Formation of a liquid phase may promote liquid phase sintering of the ZrO_2, which could decrease porosity of the scale and reduce the rate of oxygen transport to the underlying ZrB_2, thereby reducing the rate of mass gain and/or the thickness of the resulting oxide scale. This paper describes the processing, mass gain characteristics, oxide scale morphology, and scale thickness for ZrB_2 ceramics containing 4 mole percent W.

Experimental Procedure

Specimens for this study were prepared from high purity (>99%) ZrB_2 powder (Grade B, H.C. Starck, Newton, MA) with an average particle size of ~2 μm. Two weight percent B_4C (Grade HS, H.C. Starck, Newton, MA) with an average particle size of 0.8 μm was added to all batches as a densification aid (30). For batches containing tungsten, four mole percent W was added in the form of WC powder (ACER, Czech Republic), which had an average particle size of ~1 μm. Hereafter, ZrB_2 ceramics that contained only B_4C as a sintering aid are referred to as "nominally pure ZrB_2" while ceramics containing four mole percent tungsten are referred to as $(Zr,W)B_2$.

Powders were mixed by dispersion, which was accomplished by ball milling the batched powders in methyl ethyl ketone (MEK) containing a dispersant (DISPERBYK-110, BYK-Chemie Co., Wesel, Germany) for 24 hours. Powders were milled in a high density polyethylene jar using WC milling media. After dispersion, one weight percent binder (Qpac-40, Empower Materials, Newark, DE) was added and the mixture was milled for an additional 24 hours. The slurry was dried by stirring at room temperature and allowing the MEK to evaporate. The dried powder cake was ground using an alumina mortar and pestle to form granules that were passed through a 50 mesh sieve. Cylindrical disks ~19 mm in diameter were formed by uniaxial pressing in a steel die at 18 MPa. The disks were further compacted by cold isostatic pressing at ~310 MPa.

Test specimens were densified by pressureless sintering in a resistance heated, graphite element furnace (3060-FP20, Thermal Technology, Santa Rosa, CA). The heating schedule has been described in detail elsewhere (30). Briefly, pellets were heated at ~10°C/min in mild vacuum (~20 Pa) to 1650°C to facilitate removal of surface oxide impurities (31). After a one hour isothermal hold, the atmosphere was switched to flowing argon (~10^5 Pa) and the pellets were heated at 10°C/min to 2050°C and held for two hours for densification. For oxidation studies, specimens approximately 3 mm by 4 mm by 5 mm were cut from the pellets.

Additional studies on liquid phase sintering of ZrO_2 with additions of WO_3 were conducted by mixing four, six, or ten mole percent WO_3 (99.995%, Aldrich, Milwaukee, WI) with ZrO_2 (99%+, Alfa, Ward Hill, MA). Pellets were compacted in a steel die at ~18 MPa and then heated to 1300°C, 1372°C, or 1500°C for four hours in air

After densification, bulk density was measured using the Archimedes' method with water as the immersion and saturating medium. Relative densities were calculated by dividing the measured bulk density by theoretical densities that were predicted from the nominal batch compositions assuming densities of 6.1 g/cm^3 for ZrB_2, 14.9 g/cm^3 for WC, and 2.5 g/cm^3 for B_4C. Phases present in the final specimens were characterized using x-ray diffraction (XRD; XDS 2000, Scintag Inc., Cupertino, CA) analysis. Lattice parameters were determined using Rietveld refinement (JADE 5.026, Material Data Inc., Livermore, CA) of XRD data. Microstructures and oxide layer thicknesses were observed using scanning electron microscopy (SEM; S-570, Hitachi, Japan) equipped with energy dispersive spectroscopy (EDS; E2V, Scientific Instruments, UK) for simultaneous chemical analysis.

Oxidation behavior was characterized using thermal gravimetric analysis (TGA) and furnace oxidation in flowing air. Mass gain was measured as a function of temperature using TGA (Netzsch STA 409C/CD, Germany), which was conducted by heating specimens at 10°C/min to 1500°C in flowing air. Isothermal oxidation studies were carried out in a $MoSi_2$-element tube furnace (Model 0000543 Rapid Temperature Furnace, CM Inc., Bloomfield, N.J.) equipped with gas-tight end caps. Specimens were placed on zirconia setters with raised ridges to minimize the contact area between the specimen and the substrate. Specimens were heated at ~5°C/min to 1500°C or 1600°C and held for one, two, or three hours in a flowing air atmosphere. After cooling to room temperature, mass was measured and specimens were sectioned to characterize the oxide layer thickness.

Results and Discussion

Liquid Phase Sintering

The potential for liquid phase sintering in the WO_3-ZrO_2 system was studied using powder mixtures. From the WO_3-ZrO_2 phase diagram, the solidus temperature for ZrO_2-rich compositions occurs at 1257°C (32). Above this temperature, ZrO_2-rich compositions should form a liquid phase containing about 70 mole percent WO_3, which will be in equilibrium with a solid phase containing about 96 mole percent ZrO_2. Based on the phase equilibria, WO_3-ZrO_2 mixtures containing four, six, and ten mole percent WO_3 were heated to 1500°C for 4 hours to look for signs of liquid phase formation and liquid phase sintering. From the fracture surfaces in Figure 1, all of the compositions

formed a two phase mixture after heating to 1500°C. The major phase consisted of rounded, darker gray particles. Analysis by EDS (not shown) revealed that the particles were primarily composed of Zr and O. In addition, the ZrO_2 particles had grown from their starting size of ~0.5 μm to nearly 20 μm in diameter. The minor phase, which was a lighter gray color, was present at the grain boundaries. Analysis by EDS showed that this phase was rich in W and O. More importantly, the minor phase appeared to wet the grains and form a thin, continuous layer that coated the grain surfaces. Based on these observations, it appeared that the addition of four mole percent WO_3 was sufficient to promote liquid phase sintering of ZrO_2.

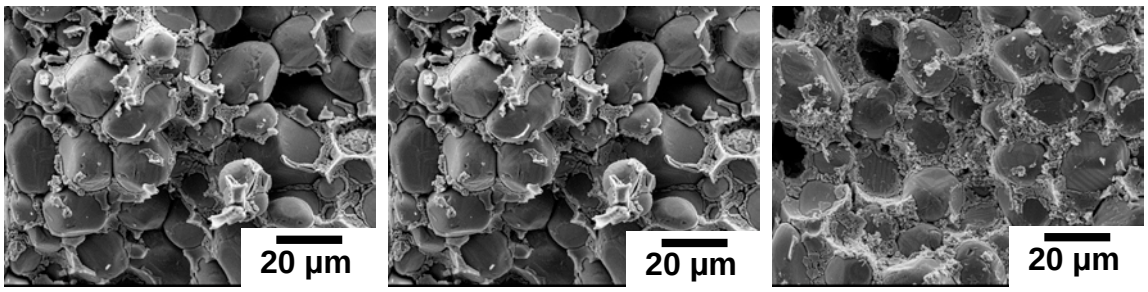

(a) (b) (c)

Figure 1. Fracture surfaces of WO_3-ZrO_2 compacts heated to 1500°C for 4 hours. The compacts contained (a) 4, (b) 6, and (c) 10 mole percent WO_3 (balance ZrO_2).

To further assess the effectiveness of WO_3 as a liquid phase sintering additive for ZrO_2, mixtures of ZrO_2 containing 4 mole percent WO_3 were heated to temperatures from 1300°C to 1500°C (Figure 2). As shown below, the lower temperatures were not effective at producing a continuous liquid phase despite the fact that both were above the solidus temperature (~1257°C). Heating to 1500°C was required to promote wetting of the ZrO_2 particles by the liquid phase. Hence, it appears that temperatures of 1500°C or higher are required to enable liquid phase sintering of ZrO_2 by a WO_3-rich liquid.

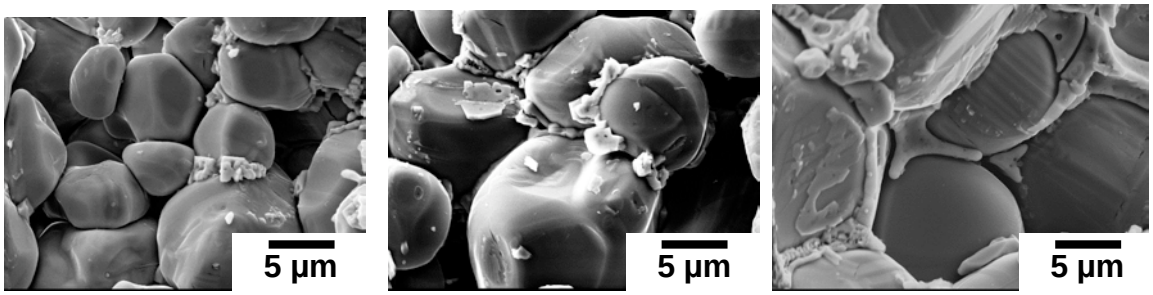

(a) (b) (c)

Figure 2. Fracture surfaces of WO_3-ZrO_2 compacts containing 4 mole% WO_3 (balance ZrO_2) heated to (a) 1300°C, (b) 1372°C, and (c) 1500°C for four hours.

Based on the liquid phase sintering studies, it was concluded that a minimum of four mole percent WO_3 would have to be incorporated into the ZrO_2 scale formed during oxidation of ZrB_2 to effectively modify scale morphology. Two ways to incorporate WO_3 into the scale were considered: 1) directly adding WO_3 to the ZrB_2 and (2) dissolving W into the ZrB_2 matrix so that WO_3 and ZrO_2 would form simultaneously during oxidation. The incorporation of WO_3 was not investigated based on the inhibiting effect that oxide impurities have on the densification of ZrB_2 ceramics. Hence, the dissolution of W into ZrB_2 was selected.

Densification, Microstructure, and Phase Analysis

Nominally pure ZrB_2 and $(Zr,W)B_2$ reached near full density after sintering at 2050°C for 4 hours. Both materials had minimal residual porosity and grain sizes of ~10 μm (Figure 3). Isolated B_4C particles, which had been added to react with and remove surface oxide impurities, were observed. Unlike B_4C, the WC that was added as a source of W in the $(Zr,W)B_2$ material was not observed after sintering. In contrast, XRD analysis revealed that diffraction peaks in specimens containing W were shifted to higher angles (30). Because W (1.4 Å) has a smaller radius than Zr (1.6 Å), (33) W could substitute onto Zr sites in the ZrB_2, which decreased its lattice parameters and shifted the XRD peaks to higher angles. Dissolution of W into ZrB_2 is consistent with the reported W_2B_5-ZrB_2 phase diagram, which indicates a W solubility of ~13 mole percent in ZrB_2 (34). Hence, SEM observations and XRD analysis are both consistent with reported phase equilibria. All indicate that W should and did dissolve into the ZrB_2 matrix.

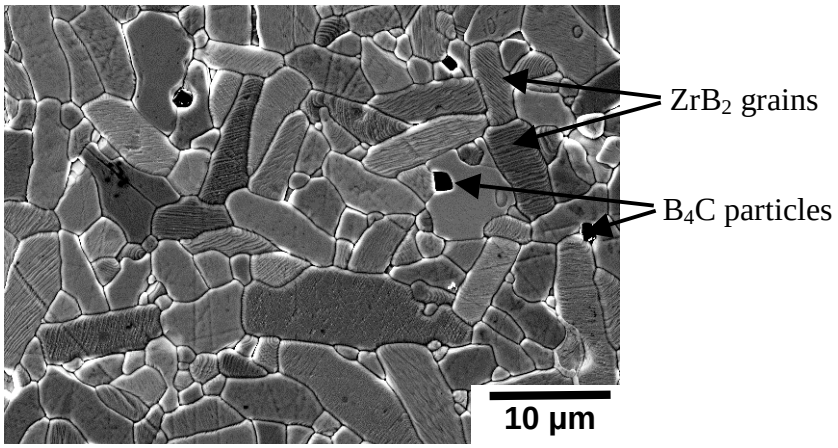

Figure 3. SEM image of a thermally etched cross section of nominally pure ZrB_2 sintered at 2050°C, which has the same grain size and shape as $(Zr,W)B_2$.

Thermal Gravimetric Analysis

Thermal gravimetric analysis showed that $(Zr,W)B_2$ had better oxidation resistance than nominally pure ZrB_2. As summarized in Table 1, $(Zr,W)B_2$ had normalized mass gain of ~4.5 mg/cm^2 after heating to 1500°C compared to ~14 mg/cm^2 for nominally pure ZrB_2. The initial mass gain for both materials started at ~700°C. However, the nominally pure ZrB_2 showed a transition to rapid mass gain at ~1200°C, which is the temperature at which B_2O_3 volatilization has been reported to become significant (18). As B_2O_3 was depleted from the oxide layer, mass gain became more significant since the porous ZrO_2 layer did not provide protection to the underlying ZrB_2. Oxidation of ZrB_2 to ZrO_2 results in a mass gain of ~10% after all of the B has been removed from the specimen by volatilization as B_2O_3. The addition of W appears to increase the temperature at which rapid mass gain begins to ~1400°C. Although the mechanism of improved protection is not evident from this experiment alone, the liquid phase sintering study described above supports the assertion that the presence of WO_3 as an oxidation product modifies the morphology of the oxide scale. Results indicate that oxidation was suppressed by better protecting the ZrB_2 from the external atmosphere. Two plausible protection mechanisms are that WO_3 acted as a liquid phase sintering aid that decreased the porosity of the scale

or that WO_3 itself acted as a barrier to oxygen transport to the underlying ZrB_2 due to the volume increase associated with oxidation of W to WO_3. In either case, the presence of W led to a significant decrease in weight gain during TGA experiments. Even though the results show that W additions were effective at improving oxidation resistance in ZrB_2, the TGA results do not reveal the full effect of W additions. Additional isothermal oxidation studies are needed to complement these results.

TABLE I. Summary of TGA results for nominally pure ZrB_2 and $(Zr,W)B_2$ for heating to 1500°C in flowing air.

Material	Onset of Mass Gain (°C)	Onset of Rapid Mass Gain (°C)	Total Mass Gain (mg/cm^2)
ZrB_2	700	1200	14.0
$(Zr,W)B_2$	700	1400	4.5

Isothermal Oxidation Studies

The addition of four mole percent W decreased the mass gain for $(Zr,W)B_2$ compared to nominally pure ZrB_2 at both 1500°C and 1600°C for oxidation times ranging from 60 to 180 minutes. For both temperatures, the decrease in mass gain was more significant at longer oxidation times (Figure 4). For example at 1500°C, the mass gain for nominally pure ZrB_2 increased from ~9 mg/cm^2 after 60 minutes to ~15 mg/cm^2 after 180 minutes. Over the same range of times at 1500°C, the mass gain for $(Zr,W)B_2$ increased from ~9mg/cm^2 after 60 minutes to ~11 mg/cm^2 after 180 minutes, which is a decrease of ~25% for the W-containing material compared to nominally pure ZrB_2. Further, the trend in mass gain for $(Zr,W)B_2$ at 1500°C suggested that W additions may lead to the formation of a protective scale since the mass gain kinetics appear to be parabolic for $(Zr,W)B_2$. This is supported by observations for specimens oxidized at 1500°C for three hours (not shown), which revealed that the thickness of the ZrO_2 scale decreased from ~500 μm for nominally pure ZrB_2 to ~100 μm for $(Zr,W)B_2$. In contrast, nominally pure ZrB_2 exhibited linear mass gain kinetics at 1500°C and 1600°C. The reduced mass gain of $(Zr,W)B_2$ at longer times may also be due to time-dependent changes in the scale morphology, which will be discussed in more detail below.

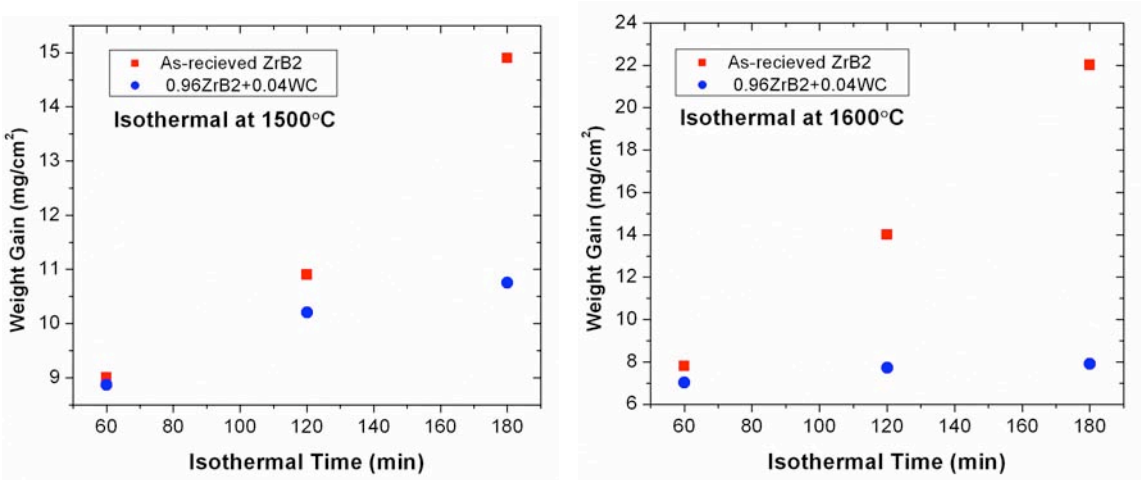

(a) (b)

Figure 4. Normalized mass gain as a function of time for nominally pure ZrB_2 (squares) and $(Zr,W)B_2$ (circles) oxidized in flowing air (a) 1500°C and (b) 1600°C. Note the difference in Y-axis scales for the two plots.

Remarkably, the oxidation protection imparted by W additions is better at 1600°C than it was at 1500°C (Table II). Whereas mass gain after 180 minutes for nominally pure ZrB_2 increased from ~15 mg/cm^2 at 1500°C to ~22 mg/cm^2 at 1600°C, mass gain for $(Zr,W)B_2$ decreased from ~11 mg/cm^2 at 1500°C to ~8 mg/cm^2 at 1600°C. So, mass gain for $(Zr,W)B_2$ decreased by ~25% when temperature increased from 1500°C to 1600°C. Although a definitive analysis of the mechanism requires more investigation, two reasonable possibilities are that W is more effective at modifying scale morphology at the higher temperature or that the WO_3-rich phase somehow becomes a more effective diffusion barrier at 1600°C.

TABLE II. Comparison of mass gain after three hours at 1500°C or 1600°C for ZrB_2 and $(Zr,W)B_2$.

Material	Mass Gain (mg/cm^2) 180 minutes at 1500°C	Mass Gain (mg/cm^2) 180 minutes at 1600°C
ZrB_2	15	22
$(Zr,W)B_2$	11	8

Combined SiC and W Additions

The mass gain of $(Zr,W)B_2$ ceramics containing 20 volume percent SiC was studied using TGA. As shown in Figure 5, the combination of SiC and W additions resulted in a lower mass gain compared to W additions alone. The onset of mass gain for all three ceramics was around 700°C. Nominally pure ZrB_2 underwent rapid mass gain above about 1200°C, resulting in a total mass gain of ~14 mg/cm^2 after heating to 1500°C. The addition of W suppressed rapid weight gain until about 1400°C, reducing mass gain to ~4.5 mg/cm^2 after heating $(Zr,W)B_2$ to 1500°C. With a combination of SiC and W additions, rapid mass gain was suppressed at temperatures below 1500°C, resulting in a normalized mass gain of less than 2 mg/cm^2. Adding a combination of W and SiC produced a silica-rich surface oxide that provided improved oxidation protection compared to the W addition alone. More detailed analysis of isothermal oxidation studies is in progress to understand the role of W in the oxidation of ZrB_2-SiC ceramics.

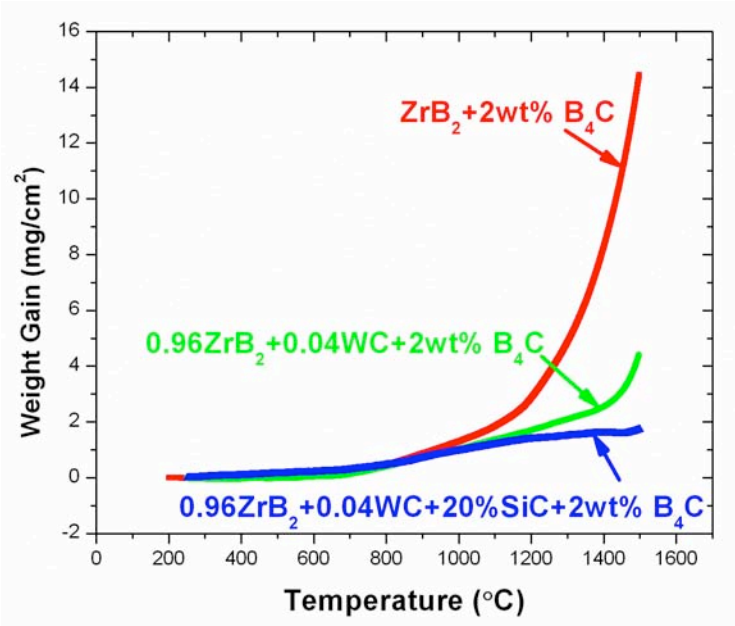

Figure 5. TGA results for nominally pure ZrB_2, $(Zr,W)B_2$ containing 4 mole percent W, and $(Zr,W)B_2$-SiC containing 4 mole percent W and 20 volume percent SiC.

Summary

Oxidation behavior was studied for ZrB_2 ceramics with W and SiC additions. Mass gain studies employing TGA showed that the addition of four mole percent W decreased mass gain from ~14 mg/cm^2 for nominally pure ZrB_2 to ~4.5 mg/cm^2 for $(Zr,W)B_2$ for heating to 1500°C in air. The beneficial role of W was further evaluated with isothermal oxidation experiments. The addition of W decreased both mass gain and oxide scale thickness compared to nominally pure ZrB_2. Remarkably, W additions appeared to provide more effective oxidation protection at higher temperatures, reducing the mass gain from ~11 mg/cm^2 for $(Zr,W)B_2$ oxidized at 1500°C for three hours to ~8 mg/cm^2 for $(Zr,W)B_2$ oxidized at 1600°C for three hours. Finally, W additions are also promising for improving the oxidation resistance of ZrB_2-SiC ceramics.

Acknowledgments

This work was funded by the Air Force Research Laboratory on contract number FA8650-04-C-5704 through the Center for Aerospace Manufacturing Technologies at the Missouri University of Science and Technology.

References

1. R.A. Cutler, in Ceramics and Glasses: Engineered Materials Handbook Volume 4, S.J. Schneider, Jr. Editor, pp. 787-803 ASM International, Materials Park, OH (1991).
2. R. Telle, L. S. Sigl, and K. Takagi, in Handbook of Ceramic Hard Materials, R. Riedel Editor, pp. 802-945, Wiley-VCH, Weinheim, Germany (2000).
3. M.J. Gasch, D.T. Ellerby, and S.M. Johnson, in Handbook of Ceramic Composites, N.P. Bansal Editor, pp. 197-224, Kluwer Academic Press, Boston (2005).
4. D.M. Van Wie, D.G. Drewry, Jr., D.E. King, and C.M. Hudson, *J. Mater Sci.*, **39** 5915 (2004).
5. Y. Murata, *U.S. Patent*, 3487594 (1970).
6. T. Kugler, *U.S. Patent*, 4376690 (1981).
7. J. Sung, D.M. Goedde, G.S. Girolami, and J.R. Abelson, *J. Appl. Phys.*, **91** 3904 (2002).
8. H.J. Ryu, Y.W. Lee, S.I. Cha, and S.H. Hong, *J. Nuclear Mater.*, **352** 341 (2006).
9. N. Kaji, H. Shikano, and I. Tanaka, *Taikabutsu Overseas*, **44** 387 (1992).
10. W.G. Fahrenholtz, G.E. Hilmas, I.G. Talmy, and J.A. Zaykoski, *J. Am. Ceram. Soc.*, **90** 1347 (2007).
11. L. Scatteia, R. Borelli, G. Marino, A. Bellosi, and F. Monteverde, in AIAA/CIRA 13th International Space Planes and Hypersonics Systems and Technologies, pp. 1-7, American Institute of Aeronautics and Astronautics, 2005.
12. J.B. Berkowitz-Mattuck, *J. Electrochem. Soc.*, **113** 908 (1966).
13. A.K. Kuriakose and J.L. Margrave, *J. Electrochem. Soc.*, **111** 827 (1964).
14. W.C. Tripp and H.C. Graham, *J. Electrochem. Soc.*, **118** 1195 (1971).
15. W.G. Fahrenholtz, *J. Am. Ceram. Soc.*, **88** 3509 (2005).
16. F. Monteverde and A. Bellosi, *J. Electrochem. Soc.*, **150** B552 (2003).
17. R.J. Irving and I.G. Worsley, *J. Less Common Met.*, **16** 103 (1968).
18. T.A. Parthasarathy, R.A. Rapp, M. Opeka, and R.J. Kerans, *Acta Mater.*, 55, 5999 (2007).

19. T.A. Parthasarathy, R.A. Rapp, M. Opeka, and R.J. Kerans, *Mater. Sci. Forum*, **595-598** 823 (2008).
20. E.V. Clougherty, R.L. Pober, and L. Kaufman, *Trans. Metall. Soc. AIME*, **242** 1077 (1968).
21. W.C. Tripp, H.H. Davis, and H.C. Graham, *Am. Ceram. Soc. Bull.*, **52** 612 (1973).
22. D. Sciti, M. Brach, and A. Bellosi, *J. Mater. Res.*, **20** 922 (2005).
23. E. Opila, S. Levine, and J. Lorincz, *J. Mater. Sci.*, **39** 5969 (2004).
24. I.G. Talmy, J.A. Zaykoski, and M.M. Opeka, *J. Am. Ceram. Soc.*, **91** 2250 (2008).
25. M.M. Opeka, I.G. Talmy, and J.A. Zaykoski, *J. Mater. Sci.*, **39** 5887 (2004).
26. M. Gasch, D. Ellerby, E. Irby, S. Beckman, M. Gusman, and S. Johnson, *J. Mater. Sci.*, **39** 5925 (2004).
27. E.J. Opila and M.C. Halbig, *Ceram. Eng. and Sci Proceed.*, **22** 221 (2001).
28. W.G. Fahrenholtz, *J. Am. Ceram. Soc.*, **90** 143 (2007).
29. S.C. Zhang, G.E. Hilmas, and W.G. Fahrenholtz, accepted for publication in *J. Am. Ceram. Soc.*, DOI: 10.1111/j.1551-2916.2008-02713.x.
30. S.C. Zhang, G.E. Hilmas, and W.G. Fahrenholtz, *J. Am. Ceram. Soc.*, **89** 1544 (2006).
31. W.G. Fahrenholtz, G.E. Hilmas, S.C. Zhang, and S. Zhu, *J. Am. Ceram. Soc.*, **91** 1398 (2008).
32. Diagram Zr-213 in *Phase Diagrams for Zirconia and Zirconia Systems*, H.M. Ondik and H.F. McMurdie, Editors, The American Ceramic Society, Westerville, OH (1998).
33. *CRC Handbook of Chemistry and Physics*, 62nd Edition, p. F-175, CRC Press, Boca Raton, FL (1981).
34. Diagram 8851 in *Phase Diagrams for Ceramists Volume X: Borides, Carbides, and Nitrides*, Anna E. McHale, Editor, The American Ceramic Society, Westerville, OH (1994).